Supporting Information

Semitransparent color tunable perovskite solar cells with 3D pillar structure

Vikas Sharma[1], Ouriel Bliah[1], Tal Binyamin[1], Shlomo Magdassi[1, *],and Lioz Etgar[1, *]

[1]The Hebrew University of Jerusalem, Institute of Chemistry, The Center for Nanoscience and Nanotechnology, Casali Center for Applied Chemistry, Jerusalem 9190401, Israel

E-mail: magdassi@mail.huji.ac.il; lioz.etgar@mail.huji.ac.il

Experimental Section

Materials: All chemicals were commercially available, procured, and used for the experiments without further purifications: Tin(IV) oxide, 15% in H_2O colloidal dispersion, Alfa Aesar), SR 9003 (ARKEMA), diphenyl (2,4,6- trimethylbenzoyl) phosphine oxide (TPO: BASF, Germany), triphenylphosphine (99%, Strem Chemicals), zinc dust (<10 μm, >98%, Sigma–Aldrich), cesium iodide (CsI: 99.999%, Sigma– Aldrich), formamidinium iodide (FAI: 99.99%, Sigma–Aldrich), lead (II) iodide (PbI_2: 99%, TCI), lead (II) bromide ($PbBr_2$: >98%, Sigma–Aldrich), Spriro- OMATEd (Sigma–Aldrich), bis (trifluoromethane) sulfonimide lithium salt (Sigma–Aldrich), and anhydrous solvents like N, N-dimethylformamide (DMF: 99.8%, Acros Organics), dimethyl sulfoxide (DMSO: 99.7%, Acros Organics), and isopropanol (>99.7%, Daejung Chemicals-Korea). The conducting PEN/ITO substrates (15 Ohm/sq) were procured from Peccell (Japan).

SnO_2 Layer Deposition: The commercially available SnO_2 nanoparticle solution was diluted by a 1:4 ratio with DI water, stirred for 30 minutes, and sonicated for 5 minutes. Before using the solution, filter it with a 0.2 μm filter. The substrate was cleaned sequentially with a soap solution, deionized water, Acetone, and isopropanol, and then dried. Before spin coating the SnO_2 solution, the samples were cleaned with plasma for 10 minutes. The tin oxide layer was deposited dynamically by spin coating at 3000 rpm for 35 s. Samples were annealed at different temperatures (60 °C for LTA and 100 °C for MTA) for 10 minutes and then immediately transferred to the plasma chamber for oxygen

plasma treatment for 10 minutes. The reference sample was annealed at 180 °C- (HTA) for 30 minutes.

Monomer-Ink Formulation: The ink is composed ofa monomer SR 9003 (Propoxylated 2 Neopentyl Glycol Diacrylate- ARKEMA Sartomer) 92 wt%, photoinitiator, TPO (Diphenyl (2,4,6- trimethylbenzoyl) phosphine oxide- BASF, Germany, 4 wt%), surface curing agent, TPP (triphenylphosphine- Strem Chemicals) 0.9 wt%, a surfactant, AFCONA-3251, AFCONA ADDITIVES (0.01 wt%), and the trifunctional acrylic monomer SR351 (Trimethylol propane Triacrylate- ARKEMA Sartomer (3 wt%). All the components were mixed well using a vortex and sonicated. The ink was kept for 24-36 hours and used to fill the printer cartridge for printing, after filtering with a 0.2 μm filter. The ink is stable for a long time (6 months) to use for printing. The viscosity of the ink is 16 Pa.s, which is suitable for inkjet printing.

Perovskite Precursor Solution: 0.5 M Perovskite ($Cs_{0.15}FA_{0.85}(PbI_{0.85}Br_{0.15})_3$) solution was prepared by the addition of CsI (19.43 mg), FAI (73.02 mg), PbI_2 (196 mg), and $PbBr_2$ (32.2 mg) into a vial with 0.8 mL DMF and 0.2 mL DMSO. The perovskite solution was stirred for 3 hours (1000 rotations per minute, at 70 °C). The prepared solution was cooled to room temperature and filtered (filter pore dia. 0.2μm) before using it.

Solar Cell Fabrication: Before the solar cell fabrication, the flexible PEN/ITO substrates with required dimensions were etched to obtain the required ITO patterns using Zn/HCl and then cleaned by placing them into a soap solution, DI water, acetone, and IPA (using an ultrasonic bath) for 10 min each. After drying with compressed air, these substrates were treated with O_2 plasma (30%, 600 s). The tin oxide layer was spin-coated and then annealed at 100°C for 10 minutes, followed by immediate treatment with oxygen plasma for 10 minutes. The 3D pillar structures were printed using an inkjet printer (OmniJet100 for DMCDPN) with solvent-free monomer and polymerized by UV light (constant illumination for 60 s, with a center wavelength of 395 nm and an intensity of 50 mW/cm²). The jetting frequency is 1000 Hz with a single-pulse waveform, and the pixel pitch is 40μm in the pixel-patterned mode of the inkjet printer. Substrate to nozzle distance is kept 3 mm, and the cartridge head (10 pL) with 16 nozzle assembly. The printing process involves purging the electrode with N2 gas to eliminate unwanted dust particles from the surface.

The printing pattern style is loaded into the software (Dimatix). Specimens were post-treated with 405 nm light for 3 minutes. After the plasma treatment, the perovskite ($Cs_{0.15}FA_{0.85}(PbI_{0.85}Br_{0.15})_3$) was spin-coated (1000 rpm for 10 s, ramp of 5 s, and 5000 rpm for 20 s, ramp of 5 s) at room temperature over the PEN/ITO/SnO$_2$/ polymer-pillared substrates. Chlorobenzene was used (10 seconds before the end of spinning) as an anti-solvent to nucleate the perovskite film. Then, the substrate was transferred onto a hot plate (110°C, 10 min). Then, 40 µL of 0.06 M 2,2′,7,7′-tetrakis-(N, N-di-4-methoxyphenylamino)-9,9′-spirofluorine (spiro-OMeTAD) in chlorobenzene with additives of 17.6 µL/1 mL bis (trifluoromethane) sulfonimide lithium salt in acetonitrile (520 mg mL−1), and 29.6 µL/1 mL of 4-tert-butylpyridine (Aldrich) was spin-coated at 4000 rpm for 40 s dynamically. Samples were left overnight in a vacuum and dark to oxidize Li salt. The top contact was deposited by thermal evaporation under high vacuum conditions. For a transparent device, MoOx (7 nm-0.1 Å/s)/Au (11 nm-1 Å/s)/MoOx (30 nm-2.0 Å/s) was deposited sequentially. For colored devices, the top MoOx thickness varied from 15-45 nm. For reference, an opaque cell with 70 nm Au was deposited using the same thermal evaporation.[1,2]

Characterization:

Morphology of the films was observed by The SEM images were acquired by using an Extra-High Resolution Scanning Electron Microscope Magellan 400L (Thermo Fisher Scientific). HV: 2KV with a current of 13pA using a TLD detector and WD: 4.5mm. Atomic Force Microscopy (AFM) measurements were performed using Dimension Icon XR Scanning Probe Microscope (Bruker, USA). Images were acquired in Tapping Mode, using RTESP-300 probes (spring constant 42 N m^{-1}, frequency 300 kHz). Raman spectrometry was measured using an InVia Confocal Raman Microscope (Renishaw). IR spectroscopy was recorded using the ATR-IR method from 400 to 4000 cm-1 on a Bruker Alpha-P machine (Bruker, USA). X-ray photo-electron spectroscopy (XPS) spectra were acquired using an XPS/UPS system (Thermo Scientific, Escalab 250Xi). The UV−Vis measurements for transmittance and absorption were recorded using the Jasco V-670 spectrophotometer. The average visible transmittance (AVT) is calculated by taking the average of the recorded transmittance values (wavelength range of 400−800 nm). During

this measurement, the reference beam is left to pass through the air for all of the devices. Photoluminescence (PL) spectra of perovskite films were obtained using a Horiba Fluoromax-4 spectrofluorometer. The device operates with a 150 W CW Ozone-free xenon arc lamp. Excitation grating of 1200 grooves mm^{-1} blazed at 330 nm. Emission grating of 1200 grooves mm^{-1}, blazed at 500 nm, and a Photomultiplier detector. Time-resolved photoluminescence (TRPL) was measured at 760 nm using a 725 nm nanoLED excitation. The average lifetime (Tavg) of the films was computed using the data obtained from curve fitting, using the equation: Tavg $=A1T1^2+A2T2^2/A1T1+A2T2$, where A1, A2 are relative amplitudes and T1, T2 are decay lifetimes. Crystal structures and phases of perovskite films were characterized using XRD measurements for the PET/SnO2/SFM-ink/perovskite substrate, which were performed on a D8 Advance diffractometer (Bruker AXS, Karlsruhe, Germany) with a secondary graphite monochromator, 2° Soller slits, and a 0.2 mm receiving slit. At room temperature, we recorded the XRD patterns within the range of 5 to 65° 2θ using Cu Kα radiation(λ = 1.5418 Å), and the measurement conditions were a tube voltage of 40 kV, a tube current of 40 mA, a step-scan mode with a step size of 0.02° 2θ, and a counting time of 1 s/step.[3–5]

Current-voltage (J-V) curves and steady-state power outputs of PSCs were measured under air mass 1.5 global (AM 1.5 G) in an ambient atmosphere. The Class AAA solar simulator was used for determining the spectral performance, uniformity of irradiance, and temporal stability. The system has a 450W xenon lamp, and the output power matched the AM1.5 global sunlights (100 mW/cm2) as the spectral match classifications were IEC60904-9 2007, JIC C 8912, and ASTM E927-05. All devices were measured by without masking the active area (0.132cm^2). J-V measurements were performed with a scan rate of 20 mV/s, ranging from 1.2 to -0.2 V and then reversed again from -0.2 to 1.2 V with a dwell time of 50 ms. EQE measurements were done using an IQE200 Newport instrument, containing a tungsten lamp for bias and a xenon lamp with a monochromator for wavelength scan. The measurements (with no-bias light or external voltage) were done in AC mode using a light chopper set at 30 Hz. Before the measurements, the EQE instrument is calibrated using a standard silicon photodiode. Charge Extraction (CE) measurements for devices were performed using an Autolab Potentiostat-Galvanostat (PGSTAT) with a FRA32M LED driver equipped with a white light source. For the data collection and analysis, we have

used the Nova 1.1 software program. During the measurement, the first step involved discharging the cell for 2 s in the dark, followed by 2 s of illumination at 0.7 suns. In the next step, the light is shut down, and the system waits for a certain time (delay time) before reconnecting and collecting the remaining charges. The measurements have several cycles, where each cycle has a different delay time between 0.5 s. Colour coordinates calculated from the reflectance spectra generated from CIE xy chromaticity diagrams. The black squares represent the experiment, while the black lines are obtained for the variation in MoOx thickness.
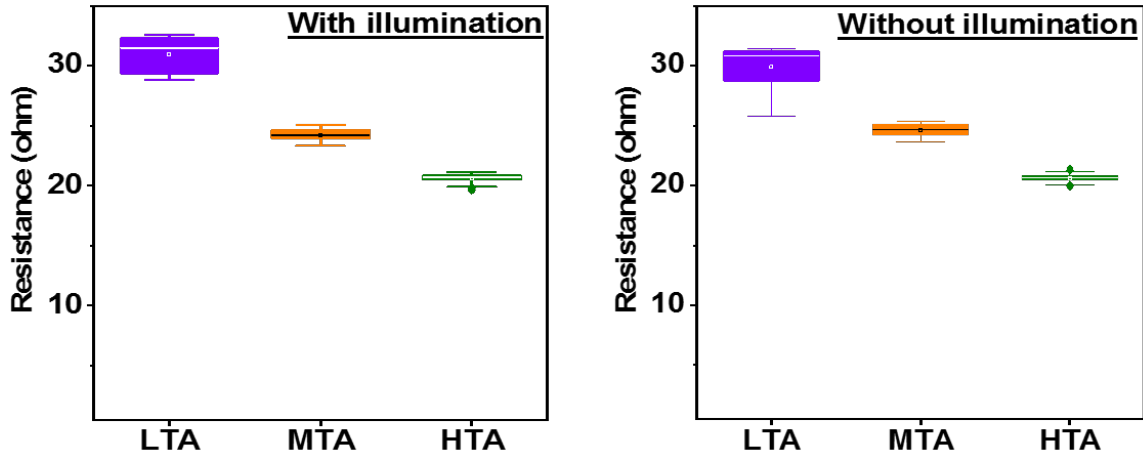
Figure S1: Resistance measurement of different SnO_2 layers measured using an ITO/SnO_2/Ag structure for LTA, MTA, and HTA layers with and without illumination.
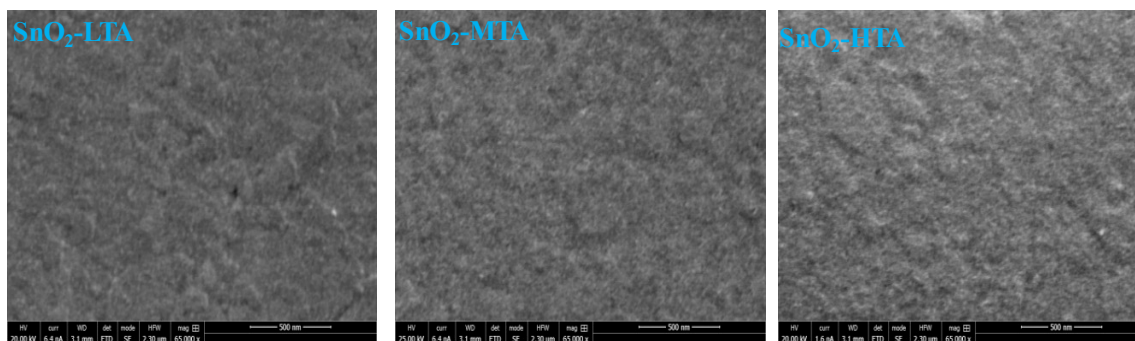
Figure S2: The surface morphological image of different SnO$_2$ layers captured by scanning electron microscopy. Here, LTA represents the 60°C annealing for 10 minutes, MTA represents 100°C annealing for 10 minutes, and subsequently 10 minutes of plasma treatment. HTA shows the samples annealed at 180°C for 30 minutes.
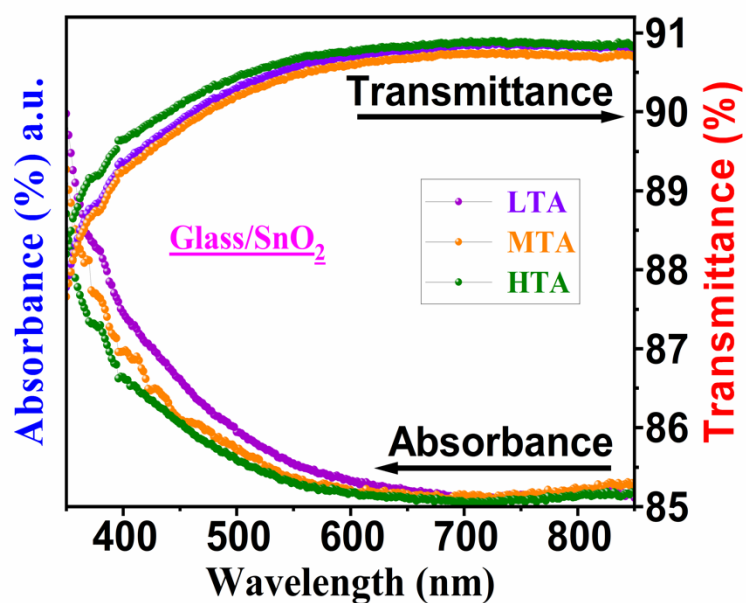
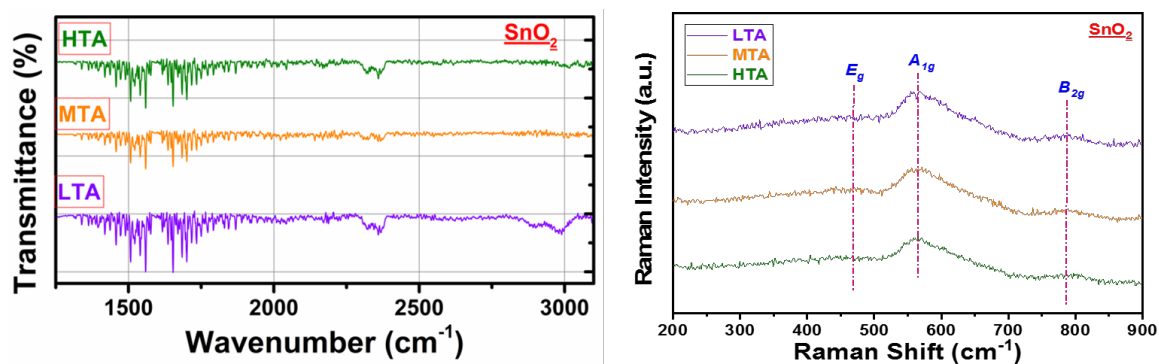Figure S3: Measured absorption and transmittance spectra of different SnO_2 layers.

Figure S4:FTIR measurement of tin oxide layers with different treatments.Raman spectra were measured using a 514 nm laser for different SnO_2layers.
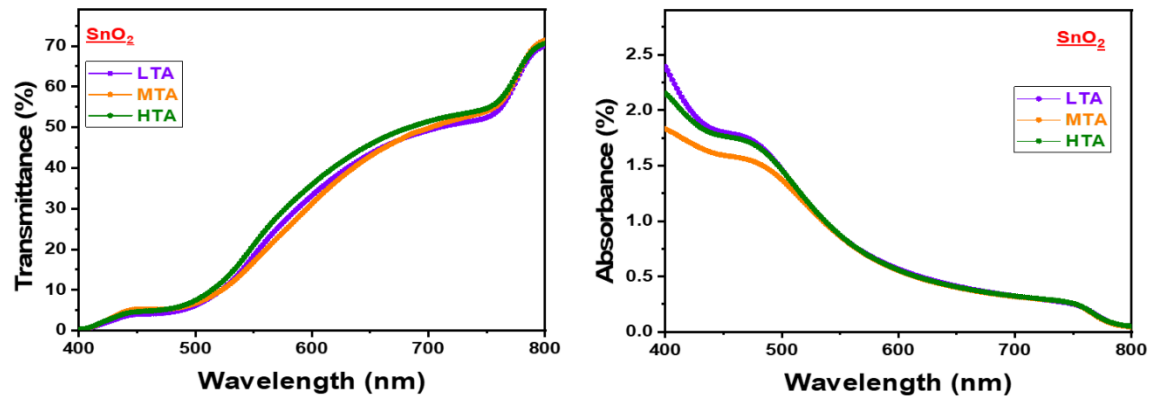
Figure S5: Transmittance and Absorption spectra of halide perovskite layer, deposited on the different SnO_2 specimens.
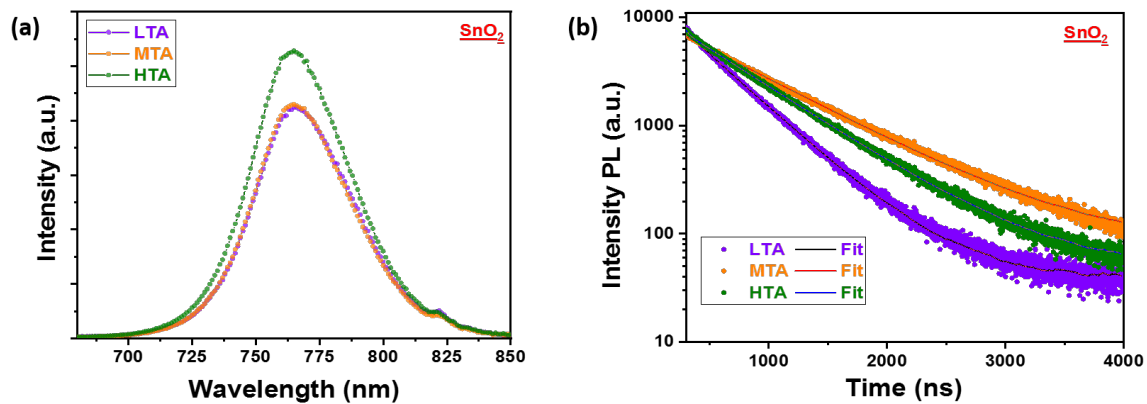
Figure S6:(a) Photoluminescence and (b) time-resolved photoluminescence spectra of $Cs_{0.15}FA_{0.85}Pb(I_{0.85}Br_{0.15})_3$ halide perovskite layer on different tin oxide films.

Table ST1: Charge carrier lifetime calculation for halide perovskite layer coated on different SnO$_2$ layers.

Specimen	$\tau 1$ (ns)	$\tau 1$ (ns)	Avg. lifetime (ns)
LTA	12.18	88.79	85.72
MTA	2.2	153	150
HTA	6.5	123	121.76

The samples were excited using 727 nm nanoLED, and measured at 760 nm using TCSPC detector. The PL-lifetime of perovskite is characterized by bi-exponential decay, in which τ_1 is related to surface recombination and τ_2 for bulk recombination. The averaged lifetime iscalculatedusing theamplitude averaged lifetime equation:

$$\tau_{avg} = \frac{\sum_i^n a_i * \tau_i}{\sum_i^n a_i}$$
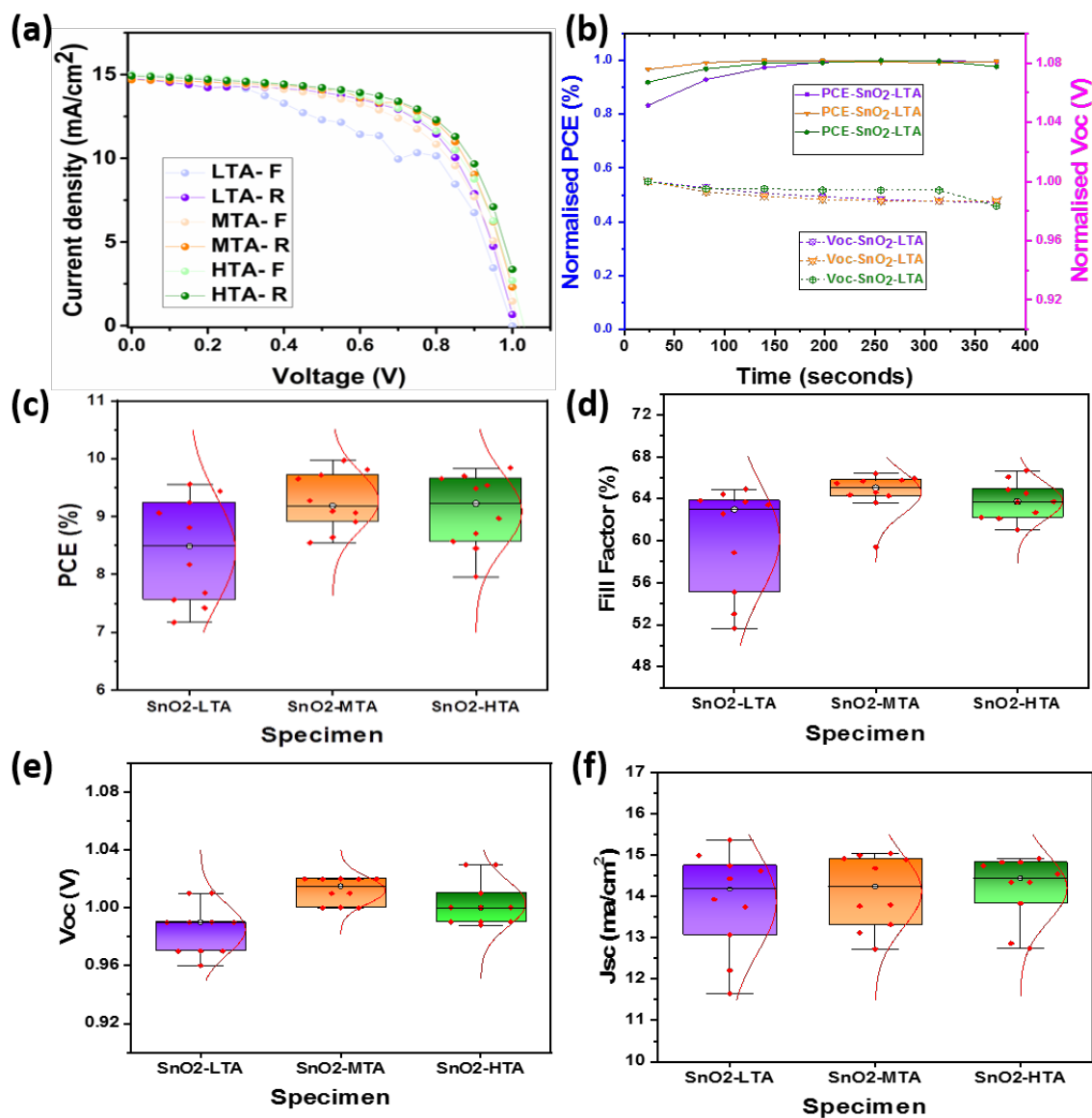
Figure S7:(a) PCE measurement of different SnO$_2$ layers. (b) Stability of the measured parameters (efficiency and open circuit voltage). Variation of 09 devices in terms of measured (c) efficiency, (d) fill factor, (e) open circuit voltage, and (f) short circuit current.
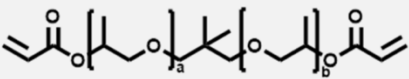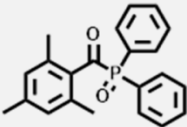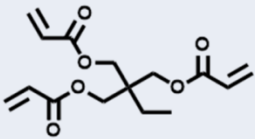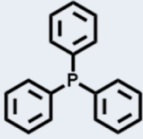
Figure S8: Chemical structure for monomer (SR 9003: Propoxylated 2 Neopentyl Glycol Diacrylate,a+b = 2), Photo initiator (TPO: Diphenyl (2,4,6-trimethylbenzoyl) phosphine oxide), Stabilizing monomer (SR 351:TrimethylolpropaneTriacrylate), and surface curing agent (TPP: Triphenylphosphine).
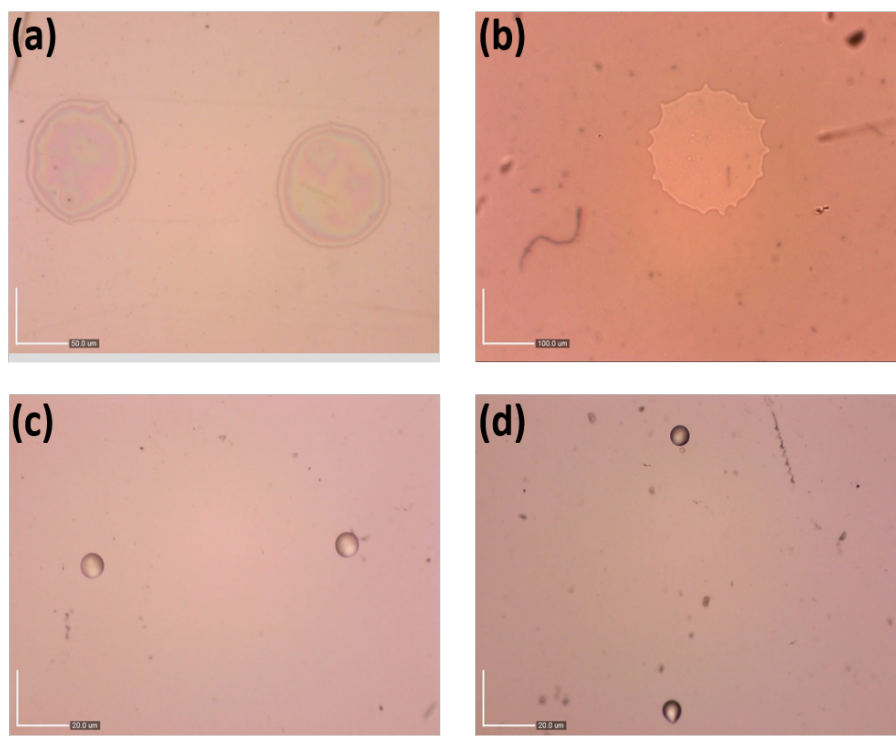
Figure S9: (a-b) optical image of the printed structure after UV curing (395 nm UV light for 1 minue) without any additive. Optical image for pillar structures obtained with two additives(c) SR- 351 and(d) AFCONA-3251.
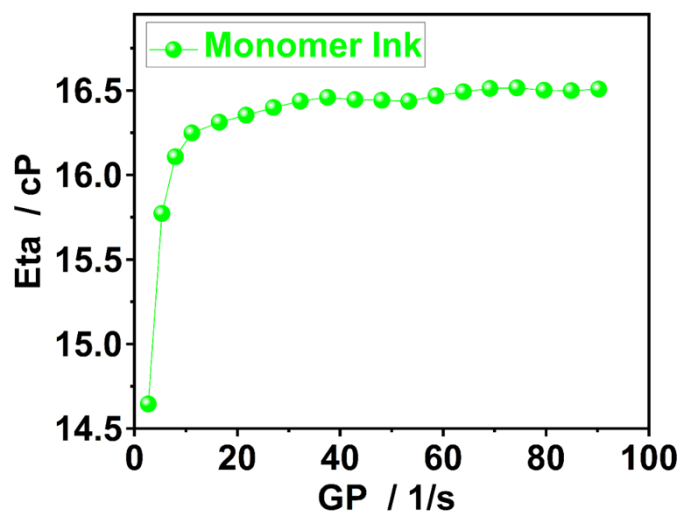

Figure S10: Viscosity plot for the monomer SR 9003 used for the ink preparation, the measurement parameters are geometry plate P60 TiL, Shear rate ranged from 0-100 (1/s), Temperature 20 degrees, Gap 0.1 (mm).
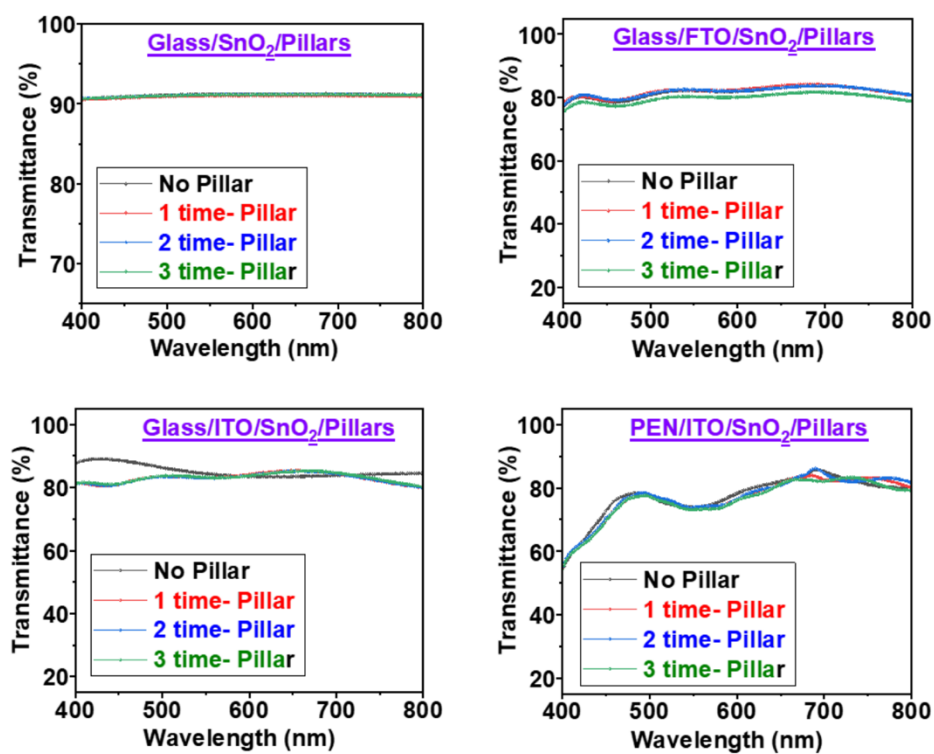
Figure S11: Optical transmittance spectra of polymer pillars on different substrates (Glass, Glass/FTO, Glass/ITO, PEN/ITO) with various number of time printing of pillar 3D structures.
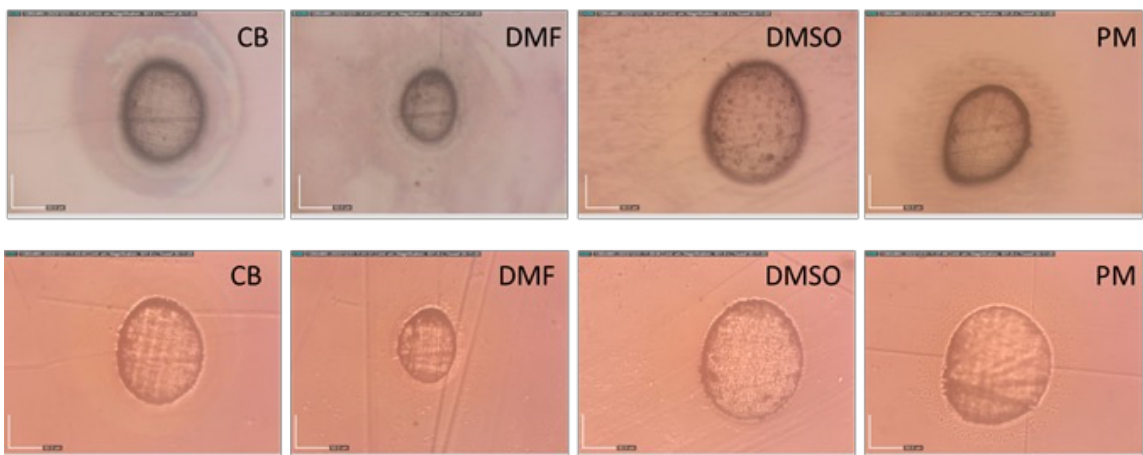
Figure S12: Optical images for pillar stability in different solvents such as chlorobenzene, DMF, DMSO, and PM solvent using optical microscope.Initial upper images show before dipping the pillars into the solvent and later one below images after the dipping. Pillar structure remain instinct with these solvents.
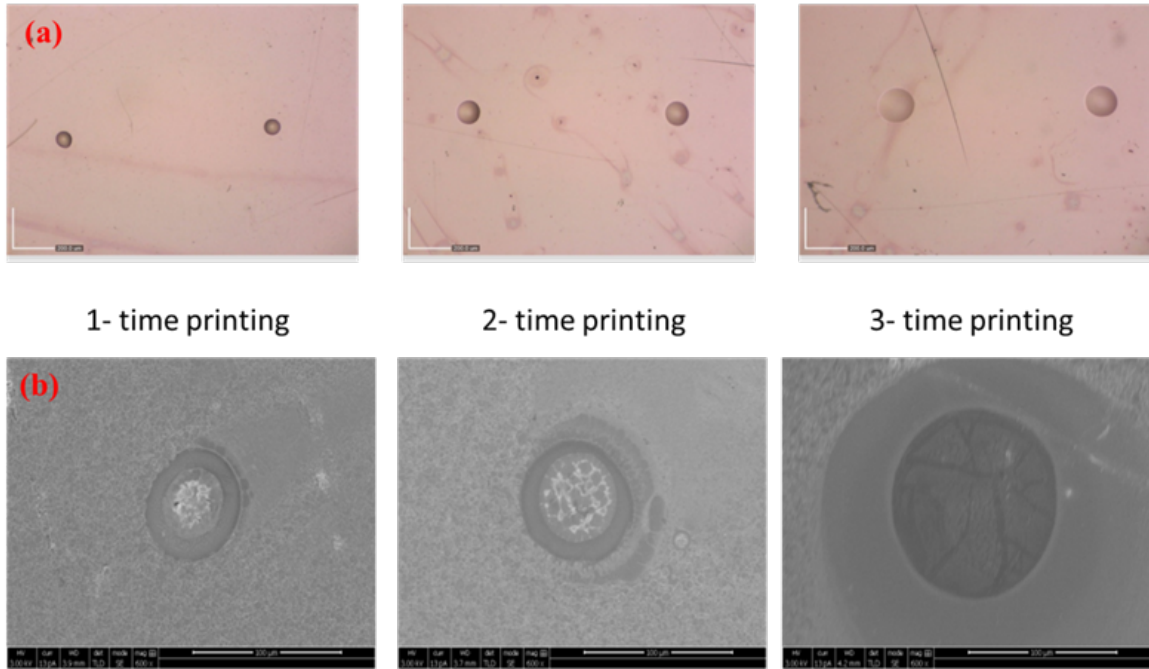
(a)

1- time printing   2- time printing   3- time printing

(b)

Figure S13:(a) Optical images of pillars, deposited on the PEN/ITO/SnO$_2$ substrate with 1-3 times in the same process to increase the size. (b) SEM images for the pillars after halide perovskite layer deposition on the different pillar sizes.
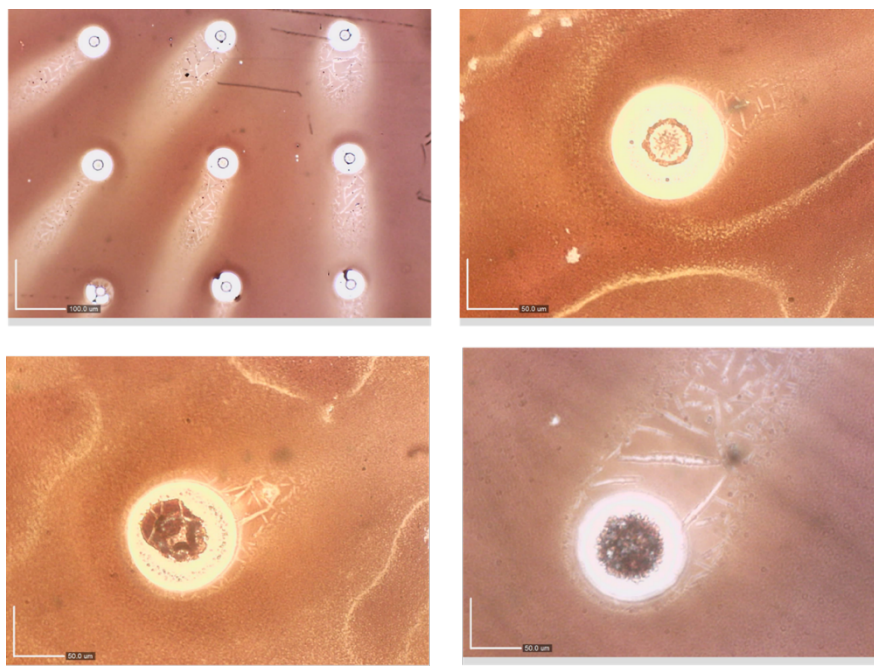
Figure S14: Top surface optical image for pillars after perovskite coating with a different number of pillars.
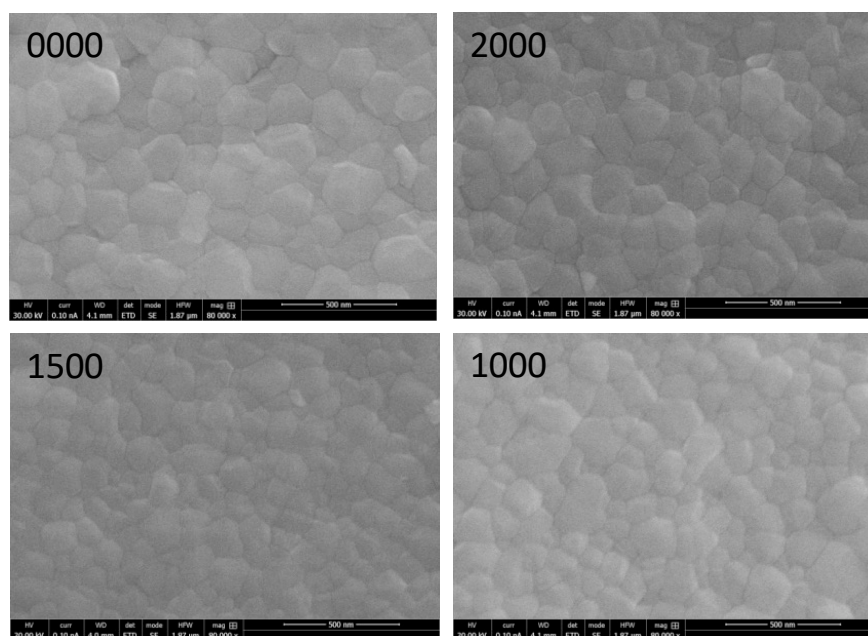

Figure S15: SEM image of halide perovskite layer between the pillars with a different number of pillars.
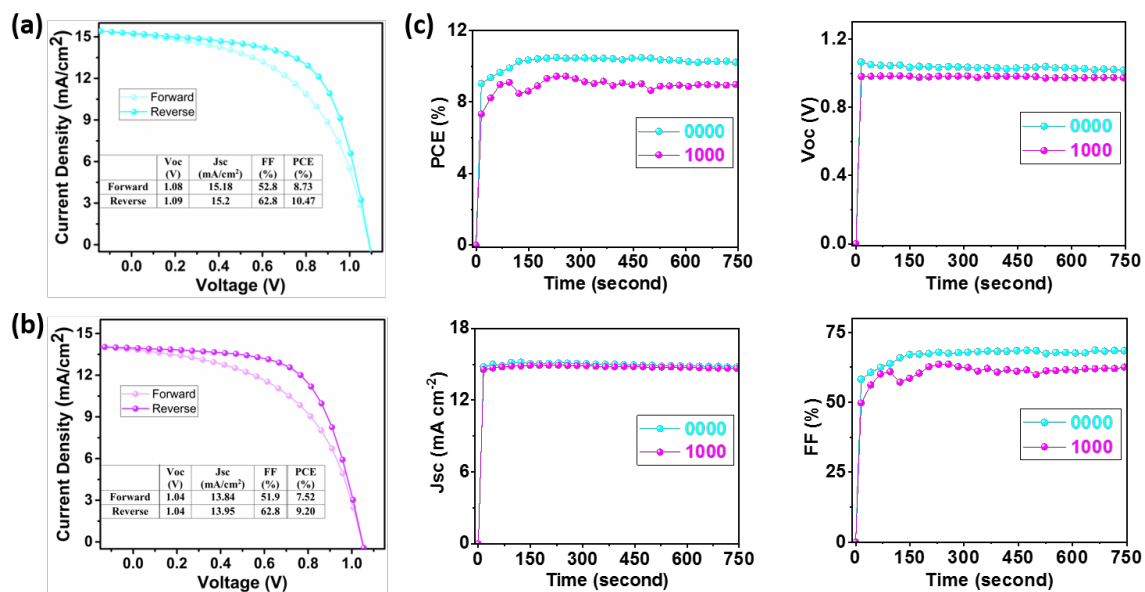
Figure S16: (a) Forward and reverse scans for no pillars and 1000 micron distance between the pillars. (c) MPPT curves for pristine and pillar embedded cell in transparent mode.

Table ST2: photovoltaic parameters for semi-transparent flexible halide perovskite cell with different amounts of pillars embedded into the perovskite.

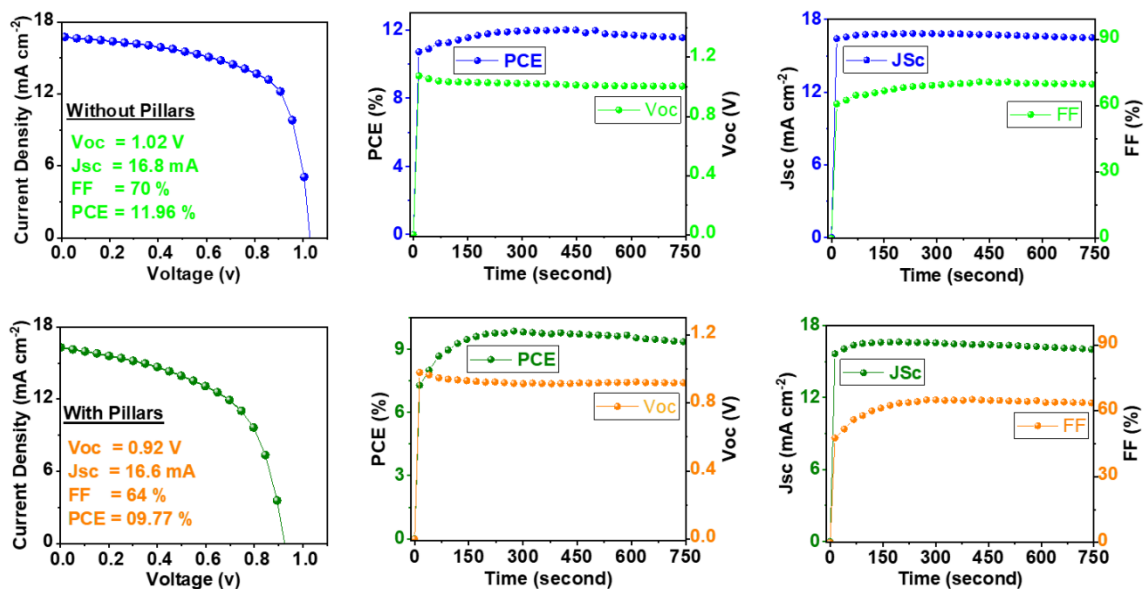| Specimen (Transparent)	Jsc (mA/cm^2)	Voc (V)	FF (%)	PCE (%)
0000	15.2	1.09	62.8	10.47
2000	14.7	1.07	66.8	10.52
1500	14.3	1.05	67.6	09.78
1000	13.9	1.04	32.8	09.20

Figure S17:J-V and Stability curve for without pillars (blue line curve) and pillar-embedded (green line curve)cells in opaque mode. The structure is PEN/ITO/SnO$_2$/Pillar (without/with)/perovskite/ Spiro/gold.

Table ST3: photovoltaic parameters for best opaque flexible halide perovskite cell without and with pillars embedded into the perovskite.

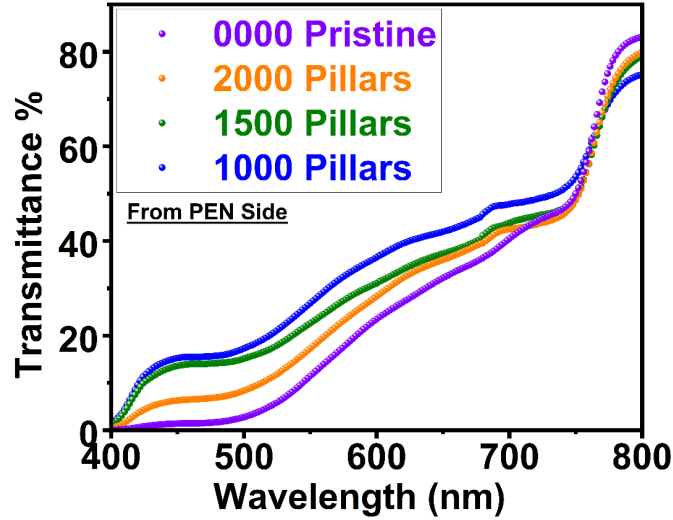| Specimen (opaque)	Jsc (mA/cm²)	Voc (V)	FF (%)	PCE (%)
0000	16.79	1.02	69.77	11.96
1000	16.58	0.92	63.79	09.77

Figure S18: Transmittance spectra of complete cell measured from the bottom transparent electrode (ITO/PEN) side with different amount of pillars embedded in the cell.

The devices were fabricated with different colours and measured for their optical and electrical behaviour. The transmittance spectra were also varied with the oxide layer thickness shown in supporting Figure S19. The reflectance spectra were also observed from the semi-transparent cells. The reflected wavelength was red-shifted with an increase in top oxide thickness from 15 to 35 nm, as shown in supporting Figure S19. There was also a change in the colour of the cell with a change in the thickness of the top MoOx layer, which can be explained based on constructive interference of specific wavelengths (corresponding to different colors in the visible spectrum) of light reflected predominantly from the air-MoOx interface and MoOx–metal interfaces. As the metal is a strong absorber of the visible spectrum, the top layer of the DMD structure forms an asymmetric Fabry-Perot cavity. Supporting Figure S20 shows this effect for different top MoOx layer thicknesses.[6] The condition for constructive interference in the asymmetric Fabry-Perot cavity thus formed is,

$$2nd cos\theta = m \lambda$$

Where n is the refractive index, d is the thickness, λ Is the wavelength, and m is an integer. Considering normal incidence of light on the films, $\theta= 0$, so $\cos\theta=1$

$$2nd = m\lambda$$

In the case of different layers (MoOx/Au/MoOx), the "nd" product depends upon the value of each layer's reflective index (n) and thickness (d).

$$nd = n_1 d_1 + n_2 d_2 + n_3 d_3 \qquad\qquad nd = \Sigma\, n_i d_i\,, \qquad \text{where "i" is the}$$

number of layers

When the thickness of the top MoOx layer changes, the change in reflected wavelength is proportional to the change in optical path length of this layer.

$$2n_1\Delta d_1 / m = \Delta\lambda$$

In the visible spectrum, the MoOx refractive index varies non-linearly between 2.4 to 3. As the impact of the wavelength dependence of the refractive index on the shift of peak reflectance was nearly three orders lower than that of the impact of change in thickness, we expect a peak shift in the range of 48 – 60 nm for a 10 nm change in layer thickness. From the reflectance curves of Figure S19, we observe that the change in the reflected wavelength was around ~ 60 nm (experimental) for a change in thickness of 10 nm (15 to 25 and 25 to 35 nm thickness) which can be shown to agree well with the theoretical calculation for the first order (m = 1) wavelength. This proves that our hypothesis about constructive interference and thickness-based color change is true. Now, we also know that from equations.

nd=n1d1+n2d2+n3d3

2nd/m=λ

So

$$\text{wavelength}\lambda = 2[\text{n1d1+n2d2+n3d3}]$$

Where m=1 (first order), n= the reflective index, and d is the thickness of respective layers, as the metal layer of the DMD structure is very thin (lower than skin depth), it is considered transparent. This will give us the value of the reflected wavelength with the concerned structure.

To confirm that the change in the color was from the variation in the oxide thickness all the changes in the DMD structure, we measured the reflectance spectra from another side of the cell. The reflectance measurement is now captured from the PEN/ITO side for the different cells with different oxide thicknesses in the top electrode, as seen in Figure S19. There was no such considerable change observed from the bottom side. The cells with different oxide thicknesses show identical reflectance spectra and visible color on the ITO/PEN side. This confirms that we can tune the color of one side of the cell with a change in the oxide thickness. Here, we must remember that color changes on the top side will show different colors with the angle/ direction of the detection. This is because of the path difference between the different reflected light and their interference. Another important thing to consider is that the oxide thickness will change the charge collection at the top electrode. Hence, we need to balance connection and oxide thickness properly.[7]

To explain this color change, we have a calculation and explanation in the previous report. Where is the change in the optical path length of this layer?

$$2n_1 \Delta d_1 / m = \Delta \lambda$$

From here we explained that the expected change/shift in the $\Delta \lambda$ should be around 60 nm which is observed experimentally (reflection peak is at ~ 455 nm (15 nm MoOx), ~ 520 nm (25 nm MoOx), ~ 580 nm (35 nm MoOx) from the reflection diagram) in line with theoretical calculations. Now, we can also calculate the reflected wavelength, which means a possible color approximation of the cells. To understand this, we need to use the same calculation shown previously. As we have three layers in our DMD Structure, so far, we also know that from the equations.

$$nd = n1d1 + n2d2 + n3d3$$

$$2nd/m = \lambda$$

So

$$wavelength\ \lambda = 2[n1d1 + n2d2 + n3d3]$$

Where m=1 (first order), n= the reflective index, and d is the thickness of respective layers, as the metal layer of the DMD structure is very thin (lower than skin depth), it is considered transparent. This will give us the value of the reflected wavelength with the concerned

structure. Here, the thickness of the bottom MoOx is 7 nm, Au is 10 nm is fixed, and the top thickness d3 changes from 15, 25, and 35 nm. The reflective index for MoOx, we can take 2.9 for lower wavelength reasons, and can calculate the wavelength, which will be similar to experimental data. This way, we can control the reflecting wavelength or, say, the color of cells. We can't go beyond a certain thickness of the top oxide layer to achieve the higher wavelength color, as this will make the contact insulating and lead to lower electrical performance of the cells. So, there should be a tradeoff between the desired color and the efficiency of the cells. By this method, we can switch the color of the cells mainly in the lower wavelength (green) side of the visible spectrum, while not so suitable for the higher wavelength (red) side.
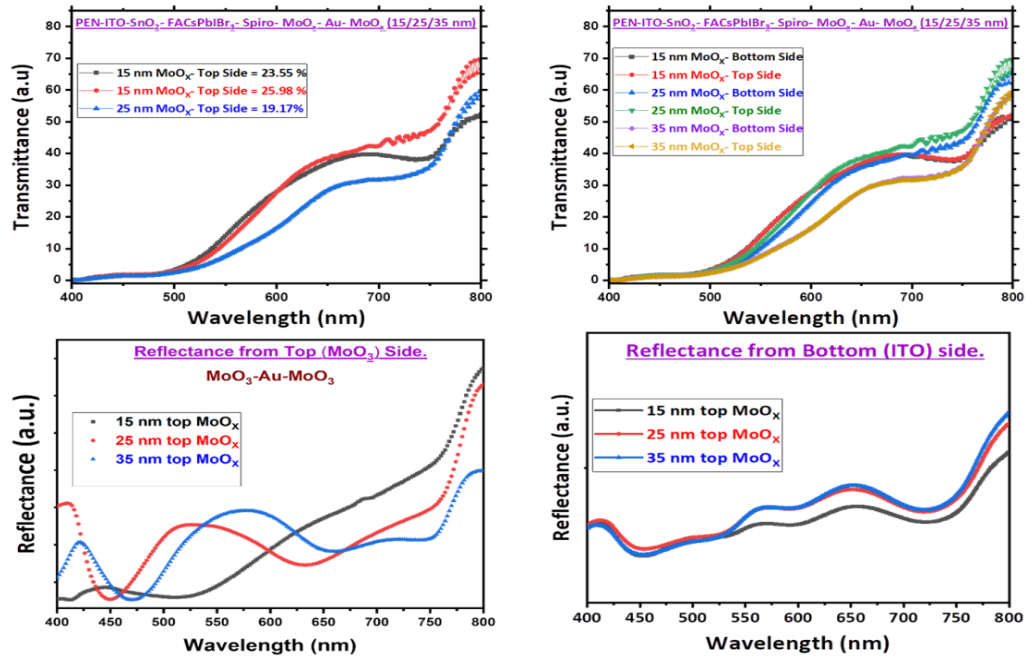

Figure S19: Optical parameter (transmittance and reflectance) curve for different colored cells measured from the top (DMD) side and bottom (ITO/PEN) side.
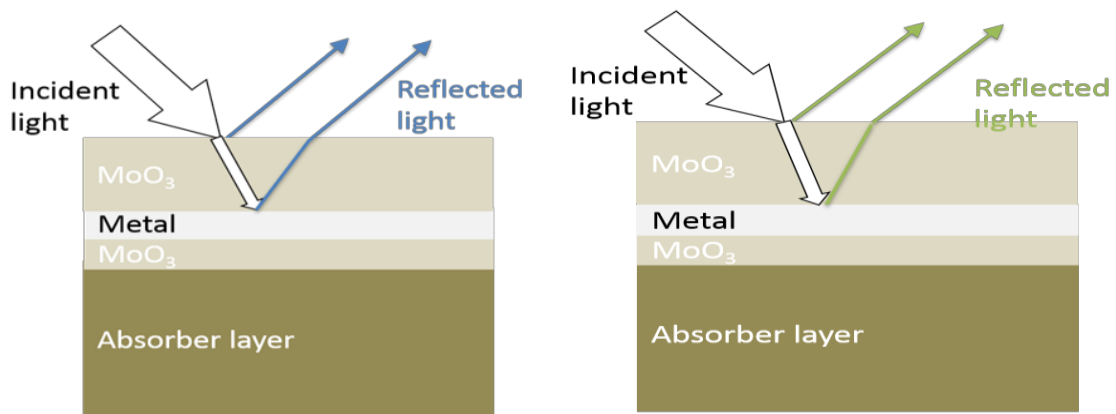
Figure S20: Graphical representation of change in the colour with change in the oxide layer thickness of the top transparent electrode.

Table ST4: photovoltaic parameters for colored, semi-transparent, flexible halide perovskite cell with different thicknesses of MoOx layer in the top transparent electrode.

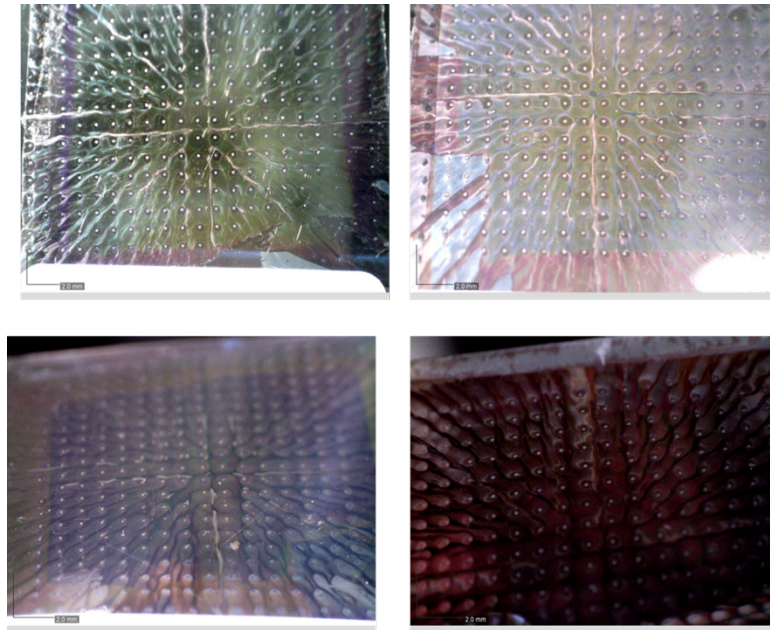| Specimen	Jsc (mA/cm²)	Voc (V)	FF (%)	PCE (%)
15 nm	11.36	0.99	60.26	6.84
25 nm	12.85	0.99	59.79	7.65
35 nm	12.64	0.97	61.72	7.57
45 nm	12.42	0.98	57.26	7.03

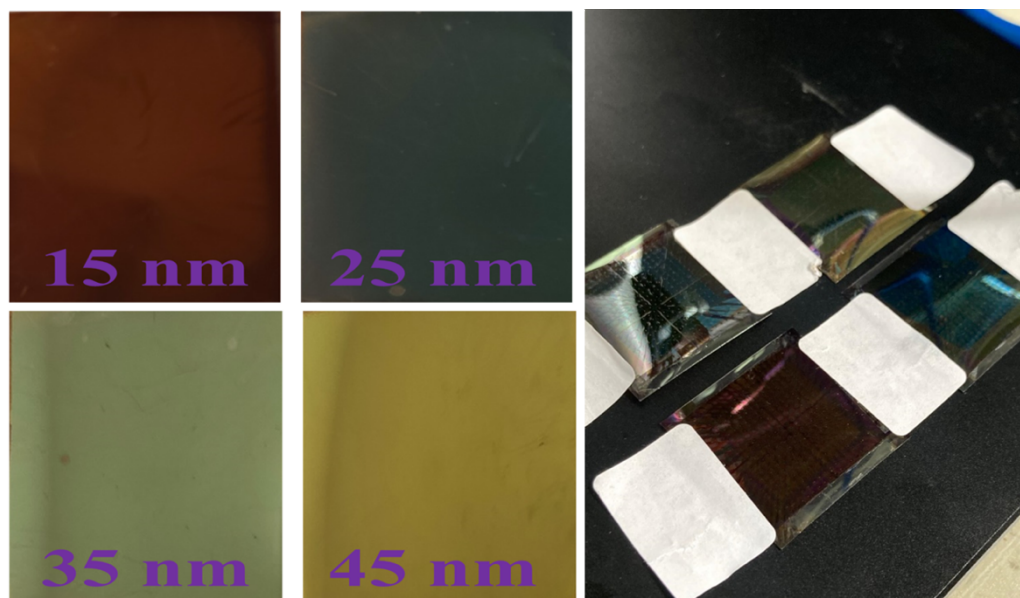Figure S21: Optical images showing the embedded pillar structures with different colour cells.

Figure S22: Camera images for different cells showing different colours with a variation of oxide thickness from 15 to 45 nm.

References:

[1]   N. K. Pendyala, S. Magdassi, L. Etgar, *ACS Appl Mater Interfaces* 2021, **13**, 30524.

[2]   M. Saliba, J. P. Correa-Baena, C. M. Wolff, M. Stolterfoht, N. Phung, S. Albrecht, D. Neher, A. Abate, *Chemistry of Materials* 2018, **30**, 4193.

[3]   T T. Wallach, L. Etgar, Appl. Phys. Rev. 2025, **12**, 011314.

[4]   C. Yang, D. Liu, M. Bates, M. C. Barr, R. R. Lunt, *Joule* 2019, **3**, 1803.

[5]   N. K. Pendyala, S. Magdassi, L. Etgar, *Sol. RRL* 2023, **7**, 2200988.

[6]   A. Lorusso, S. Masi, C. Triolo, F. Mariano, S. Muia, A. Cannavale, Y. Duan, M. Anni, M. L. De Giorgi, S. Patané, O. Selmi, I. Mora-Seró, S. De Leo, M. Mazzeo, *ACS Energy Lett* 2024, **9**, 1923.

[7]   J J. Heo, I. Jung, H. Park, J. H. Han, H. Kim, H. Park, J. S. Park, H. Jeon, K. T. Lee, H. J. Park, *Adv. Opt. Mater.* 2022, **10**, 2101696.